FABRICATION, TREATMENT, AND TESTING OF MATERIALS AND STRUCTURES

Controlled Growth of One-Dimensional Zinc Oxide Nanostructures in the Pulsed Electrodeposition Mode

N. P. Klochko[a]^, G. S. Khrypunov[a], Yu. O. Myagchenko[b], E. E. Melnychuk[b], V. R. Kopach[a], E. S. Klepikova[a], V. N. Lyubov[a], and A. V. Kopach

[a]*National Technical University "Kharkiv Polytechnical Institute", ul. Frunze 21, Kharkiv, 61002 Ukraine*
^e-mail: klochko_np@mail.ru
[b]*Taras Shevchenko National University of Kyiv, ul. Volodymyrska 62, 03680 Kyiv, Ukraine*
Submitted November 15, 2011; accepted for publication November 21, 2011

Abstract—Zinc oxide nanostructures are objects of study in the field of optoelectronics, solar power engineering, nanosensorics, and catalysis. For the purpose of the controlled growth of one-dimensional submicrometer zinc oxide structures in the pulsed electrodeposition mode, the effect of the pulse electrolysis parameters on the morphology of ZnO layers, their optical properties, and structural and substructural characteristics is determined using X-ray diffraction, optical spectrophotometry, and atomic-force microscopy. The possibility of fabricating arrays of ZnO nanowires with different geometrical shapes, perpendicular to the substrate surface, by varying the frequency of cathode–substrate potential pulses is shown.

1. INTRODUCTION

Due to unique optical and electrical properties and inclination toward the formation of one-dimensional (1D) submicrometer filamentary structures, i.e., nanowires, nanorods, nanoribbons, and nanotubes, zinc oxide (ZnO) is an object of extensive studies in the field of optoelectronics, solar power engineering, nanosensorics, and catalysis. In addition to such expensive methods for growing zinc oxide filamentary crystals as explosive laser deposition [1] and high-frequency vacuum sputtering [2], increasing interest is being drawn to highly efficient and inexpensive chemical [3] and physicochemical methods, among which the electrochemical cathode deposition of ZnO nanocrystallite arrays on conductive substrates from aqueous solutions is most widely accepted [4–11]. This is because zinc oxide nanostructure growth using this method combines such advantages as simple processing equipment and applicability to mass production, and process controllability which is very important in the fabrication of optoelectronic devices, gas nanosensors, organic solar cells, and hybrid photoelectric converters (dye-sensitized solar cells, DSSCs). To impart the necessary morphology to the ZnO nanostructures, the effect of the cathode potential [4], electrolyte composition [10], deposition temperature and time, the presence of various organic additives and complexons [5, 6], subsequent hydrothermal processing [7], annealing [11], and even gravitation [9] on the structure and properties of the grown arrays of submicrometer zinc oxide elements is actively studied. In this case, the electrolysis process is performed under potentiostatic conditions, i.e., at a constant cathode potential; very few studies are carried out using electrodeposition under conditions of pulsed cathode potential variations. For example, pulsed electrodeposition was used in [8] to fabricate zinc oxide nanowires doped with copper and manganese; however, that study was focused on growth control using the pulsed electrolysis mode by varying dopant contents, rather than on the surface morphology. At the same time, in previous studies of the cathodic electrodeposition of copper and indium diselenide [12], we showed that pulse electrolysis, in particular, can provide the controlled growth of semiconductor nanostructures without their possible contamination by organic or other impurities from an electrolyte. Later on [13], we showed that the preferential growth of zinc-oxide nanocrystal arrays of the wurtzite modification in the direction perpendicular to the substrate surface, i.e., along the crystallographic C axis, can be provided by preventing gaseous hydrogen adsorption on the (001) plane, which occurs during cathodic electrochemical deposition of ZnO. To this end, pulse electrolysis with rectangular pulses of the cathode potential should be used. The objective of this study is to determine the effect of the pulse electrolysis parameters on the morphology, structural parameters, and optical properties of ZnO layers to implement the controlled growth of 1D submicrometer zinc oxide structures in the pulsed electrodeposition mode.

2. EXPERIMENTAL

Arrays of zinc oxide nanoelements were fabricated by cathodic electrochemical deposition in a three-

electrode electrochemical cell with not mixed aqueous electrolyte containing 0.05 M $Zn(NO_3)_2$ and 0.1 M $NaNO_3$ at a temperature of 70°C. Glass plates coated with transparent conductive layers of fluorine-doped tin oxide (SnO_2:F, or FTO, Pilkington Corp., USA) were used as the substrates (cathodes, or working electrodes). A platinum spiral was used as a counter electrode; a saturated silver-chloride electrode Ag/AgCl was used as a reference electrode. To implement the potentiostatic electrodeposition mode, a constant cathode potential $U = -1.1$ V was maintained by a PI-50-1.1 pulsed potentiostat with a PR-8 programmer (hereafter, the potentials are measured relative to the silver-chloride electrode). Samples were prepared by the pulse electrolysis method by applying rectangular potential pulses to the cathode substrate, so that the lower and upper potential limits were $U_{off} = -0.8$ V and $U_{on} = -1.4$ V. Thus, the variation amplitude of the cathode potential during pulse electrolysis was 0.6 V. The pulse ratio Q, i.e., the ratio of the total pulse and pause duration to the pulse duration, was 2.5 in all cases. The pulse frequency (from 1 to 200 Hz) during the electrodeposition of each individual sample remained constant over one hour.

The optical properties of the arrays of zinc oxide nanocrystallites were studied in the spectral range of 350–850 nm using an SF-46 spectrophotometer. FTO/glass substrates (Pilkington Corp., USA) were used as reference samples when measuring the optical transmittance T spectra. The optical band gap E_g of the zinc oxide layers was determined using the relation [14]

$$\alpha = \frac{A(h\nu - E_g)^n}{h\nu}, \qquad (1)$$

where A is a constant, which depends on the carrier effective mass in a material; $h\nu$ is the optical-photon energy; α is the absorbance of a semiconductor layer with the thickness d_0; $\alpha = -(1/d_0)\ln T$; and n is an exponent controlled by the photon absorption mechanism in the semiconductor.

The band gap of the direct-gap semiconductor, which is ZnO [14], was determined by extrapolating the linear portion of the dependence $(\alpha h\nu)^2$ on $h\nu$ to the energy axis. If it was difficult to determine the zinc oxide layer thickness, e.g., as in the case of 1D nanocrystal formation, E_g was determined according to [5] by extrapolating the linear portion of the dependence $[(-\ln T)h\nu]^2$ on $h\nu$ to the energy axis.

The structural disorder of the electrodeposited layers of zinc oxide was estimated according to [15] by the Urbach energies E_0, proceeding from the fact that the absorbance near the band gap is characterized by an exponential dependence on the photon energy,

$$\alpha = \alpha_0 \exp\left(\frac{h\nu}{E_0}\right), \qquad (2)$$

where α_0 is a constant.

In the absence of data on the thickness of the electrodeposited arrays of zinc oxide nanostructures, the Urbach energy was determined by the slope of the linear portion of the dependence $\ln[-\ln(T)]$ on $h\nu$.

To analyze the layer structure, X-ray spectra were measured using a DRON-4 diffractometer in CoK_α radiation (the wavelength is $\lambda = 1.7889$ Å). Scanning was performed in the angular range $2\theta = 30°-80°$ with Bragg–Brentano focusing ($\theta-2\theta$). The measured X-ray diffraction patterns were processed (background separation, $K_{\alpha1}-K_{\alpha2}$ doublet splitting, and others) and the parameters of the profile of the diffraction line were calculated using the New_Profile 3.4 (486) and OriginPro 7.5 software packages. The presence of crystalline phases was detected by comparing the data obtained from experimental X-ray diffraction patterns with the JCPDS database using the PCPDFMIN 1.30 software package. The sizes of the grains L, coherent-scattering regions (CSRs), and microstrains $\Delta d/d$ (where d is the crystal lattice parameter according to JCPCDS; Δd is the difference between the experimental and reference values for the crystal lattice parameter) in the arrays of zinc oxide nanostructures were estimated by analyzing the broadening of the X-ray diffraction maxima, taking into account instrumental broadening by the Scherrer equation [8] and the Williamson–Hall approximation [16, 17], respectively. The crystal lattice parameters a and c of the hexagonal phase of zinc oxide were calculated by the position of the last two indexed lines of the X-ray diffraction patterns according to [8]. The texture of the electrodeposited arrays of zinc oxide nanostructures was studied using the total intensities of the diffractometric peaks I_i. For each peak, the pole density P_i characterizing the probability of the coincidence of the normal to the crystallite surface and the normal to the (hkl) plane, i.e., defining the number of crystallites in which the (hkl) planes are parallel to the sample surface, was calculated by the ratio [18]

$$P_i = \frac{(I_i/I_{0i})N}{\sum\limits_{1}^{N} I_i/I_{0i}}, \qquad (3)$$

where I_{0i} is the total intensity of the ith diffractometric peak according to the JCPDS data and N is the number of diffractometric peaks.

The pole densities were determined for all peaks in the X-ray diffraction patterns; the value $P_i > 1$ was assigned to the texture axis.

The surface morphology of the zinc oxide layers was studied by intermittent-contact atomic-force microscopy (AFM) using a NanoLaboratoriya Integra Prima NT-MDT setup.
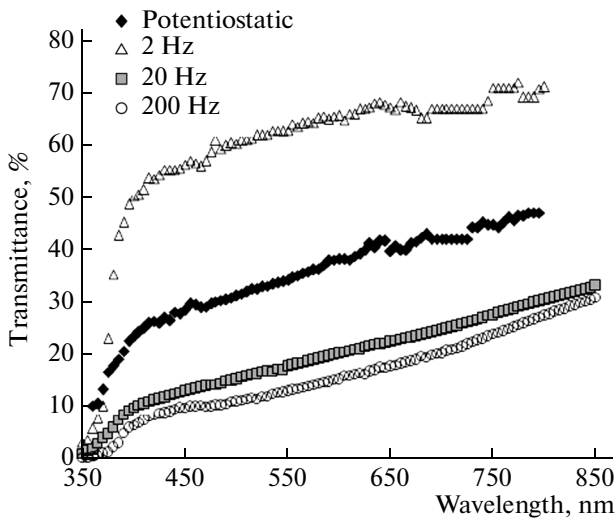
Fig. 1. Optical transmittance spectra of ZnO layers electrodeposited in the potentiostatic and pulse modes.

Fig. 2. Dependences of $[(-\ln T)h\nu]^2$ on the photon energy for ZnO layers deposited in the potentiostatic and pulse modes.

3. EXPERIMENTAL RESULTS

3.1. Optical Properties

The electrodeposited ZnO films were semitransparent, exhibited significant diffuse scattering of light, and looked whitish in reflected light. An exception was a sample fabricated in the pulse electrolysis mode at the frequency $f = 2$ Hz, which was almost transparent. The study of the optical transmission spectra in the visible region (Fig. 1) showed that the maximum optical transmittance of arrays of zinc oxide nanocrystallites fabricated in the potentiostatic electrolysis mode reached $T = 46\%$, and the transparency of the arrays of zinc oxide nanocrystallites grown in the pulse electrolysis mode depended on the pulse frequency, decreasing with f. The band gap E_g for direct optical transitions of ZnO layers deposited in the potentiostatic and pulse modes was within $3.01-3.23$ eV (Fig. 2), which correlates well with the published data for bulk zinc oxide samples [10]. The study of the dependences $[-\ln(T)h\nu]^2$ on $h\nu$ showed that the absorption edge has no distinct boundary and increases exponentially with the photon energy according to the Urbach rule [15]. The dependences shown in Fig. 3 contain a flat portion at energies near E_g, associated with imperfection in the zinc oxide structure, which causes the appearance of exponentially distributed states at band tails and results in the dominance of optical transitions involving these states near the absorption band edge. The band tail's slope is controlled by the Urbach energy E_0 depending on the degree of structural disorder in the zinc oxide layers, thus being a measure of this disorder. As calculations showed, the narrowest band gap and the least ordered structure are inherent to ZnO layers deposited in the potentiostatic mode ($E_g = 3.01$ eV, $E_0 = 0.83$ eV). We can see in Fig. 4 that the band gap tends to decrease, and the Urbach energy
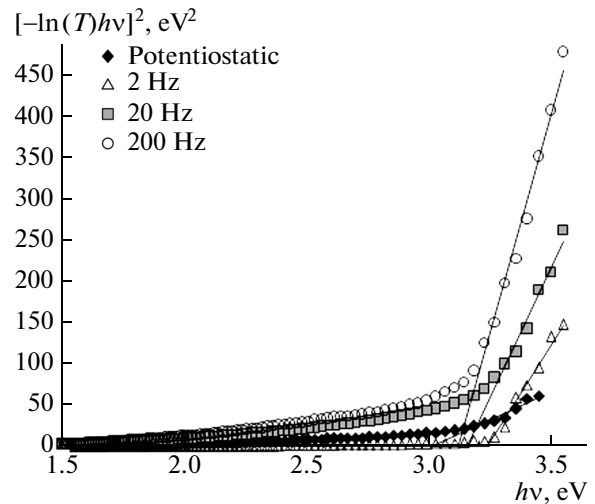
tends to increase with the pulse frequency, although not monotonically, in the case of the pulse deposition of zinc oxide. In general, we can state that there is significant structural ordering of ZnO nanocrystallite arrays fabricated in the pulse mode in comparison with those grown at the constant cathode potential.

3.2. Structure

The X-ray diffractometry study of the structure and phase composition of the electrodeposited zinc oxide layers showed that all diffraction peaks, except for those related to the FTO/glass substrates, correspond to the hexagonal wurtzite-type ZnO modification (Fig. 5). The structural and substructural parameters
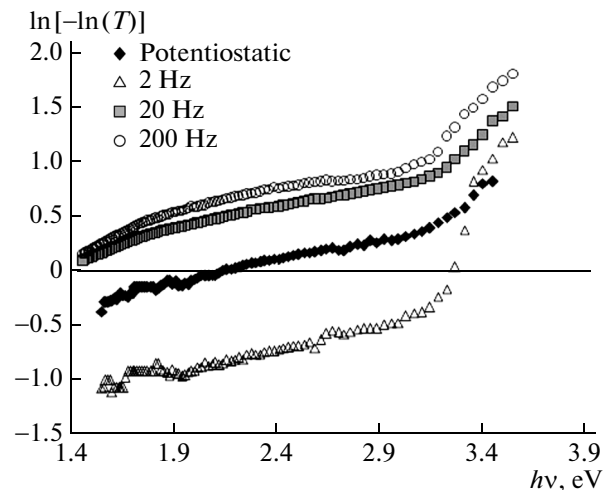

Fig. 3. Dependences of $\ln[(-\ln T)]$ on the photon energy for ZnO layers deposited in the potentiostatic and pulse modes.
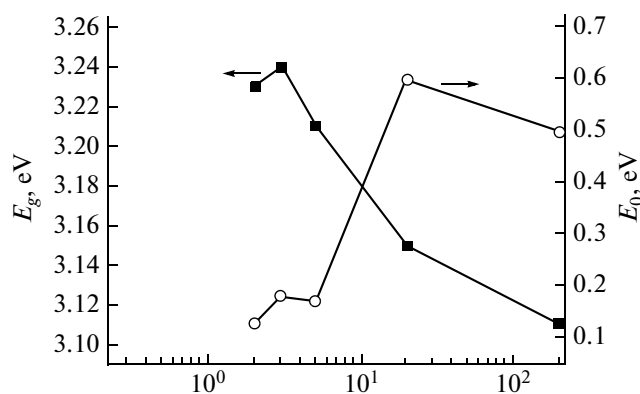
Fig. 4. Dependences of the band gap and Urbach energy on the potential pulse frequency during zinc oxide layer deposition.

Fig. 5. X-ray diffraction patterns of ZnO layers deposited on FTO/glass substrates in the potentiostatic and pulse modes.

of the electrodeposited zinc oxide layers, calculated using the X-ray diffraction data are listed in the table. We can see that the average sizes of crystallites L and coherent-scattering regions (CSRs) are 100–200 nm. Unfortunately, it was impossible to apply approximations to separate the size and strain contributions to broadening of the diffraction maxima for the samples deposited at low frequencies ($f = 1–5$ Hz), since the calculated CSRs exceeded the values permissible within the context of this method. Therefore, the table contains no data on microstrains and CSRs in the ZnO layer deposited at a frequency of 2 Hz. In general, the analysis of the X-ray diffraction data allows the conclusion that zinc oxide layers deposited in the potentiostatic and pulse modes are nanostructured. The ZnO nanocrystallite arrays deposited at a constant substrate potential and potential pulse frequencies $f = 1–20$ Hz are characterized by insignificant microstrains. The significant broadening of diffraction peaks in the case of the sample deposited at the pulse frequency of 200 Hz is attributed to both anomalously large crystallite dispersity and increased microstrains in the ZnO layer.

The crystal lattice parameters a of the deposited ZnO films, calculated according to [18], are close to the reference data JCPDS No. 36-1451 ($a = 3.249$ Å).
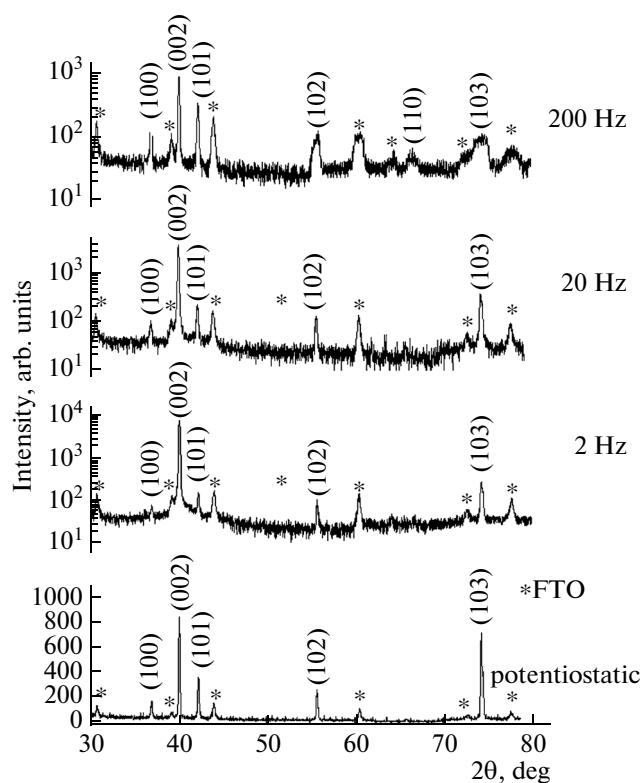
At the same time, the lattice parameter c determined in the zinc oxide layers that were grown in the potentiostatic mode and pulse electrodeposition modes at low frequencies ($f = 1–20$ Hz) is larger than the reference one (according to JCPDS No. 36-1451, $c = 5.207$ Å), which suggests that the structure of zinc oxide elements is extended along the c axis, which is typical of filamentary crystals. In contrast, in the layers deposited at the frequency $f = 200$ Hz, the lattice parameters are close to the reference ones.

Our interest in the texture of the electrodeposited ZnO layers was explainable by the circumstance that, according to [19], an increase in the relative intensity

Structural and substructural characteristics of electrodeposited ZnO layers

Electrodeposition conditions [mode?]	Texture direction, pole density P_{hkl}	L, nm [8]	CSR, nm [16, 17]	Microstrains $(\Delta d/d) \times 10^3$ [16, 17]	Lattice parameters, Å	
					a	c
Potentiostatic	$\langle 103 \rangle$, 1.88	135	130	0.3–1.1	3.257	5.221
	$\langle 001 \rangle$, 1.46					
Pulse, $f = 2$ Hz	$\langle 001 \rangle$, 4.52	206	–	–	3.256	5.218
Pulse, $f = 20$ Hz	$\langle 001 \rangle$, 3.12	156	120	0.3–0.6	3.253	5.220
Pulse, $f = 200$ Hz	$\langle 001 \rangle$, 2.01	160	40	6.4–7.9	3.250	5.206
	$\langle 103 \rangle$, 1.45					

P_{hkl}

entation in the (103) and (002) planes. At the same time, the layers grown in the pulse electrolysis mode at frequencies of 1−20 Hz have significant preferred orientation of structural elements in the (002) plane, i.e., are textured along the C axis perpendicular to the substrate surface. The frequency dependence of the pole density for the (002) texture has a maximum at $f = 2$ Hz (Fig. 6). As the pulse frequency further increases, the fraction of crystallites with texture in the (001) direction decreases. The zinc oxide nanocrystallite array grown at a frequency of 200 Hz has two insignificant preferred orientations in the (002) and (103) planes.

Fig. 6. Dependence of the pole density on the pulse frequency for ZnO layers textured in the ⟨001⟩ direction.

3.3. Surface Morphology

The use of atomic-force microscopy not only provided visualization of the ZnO structure layers, but also promoted interrelation of the electrolysis modes, morphology of the electrodeposited zinc oxide layers, and the data of optical and structural studies. Figure 7a shows the image of the structurally disordered untextured nanograin film deposited in the potentiostatic mode. Figures 7b and 7c show the arrays of 1D nanostructures perpendicular to the substrate surface, which were grown in the pulse deposition mode at frequencies of 2 and 20 Hz, respectively. In this case, the most structurally ordered, according to the data of optical studies, and the most textured in the (002) plane, according to the results of X-ray diffraction, zinc oxide
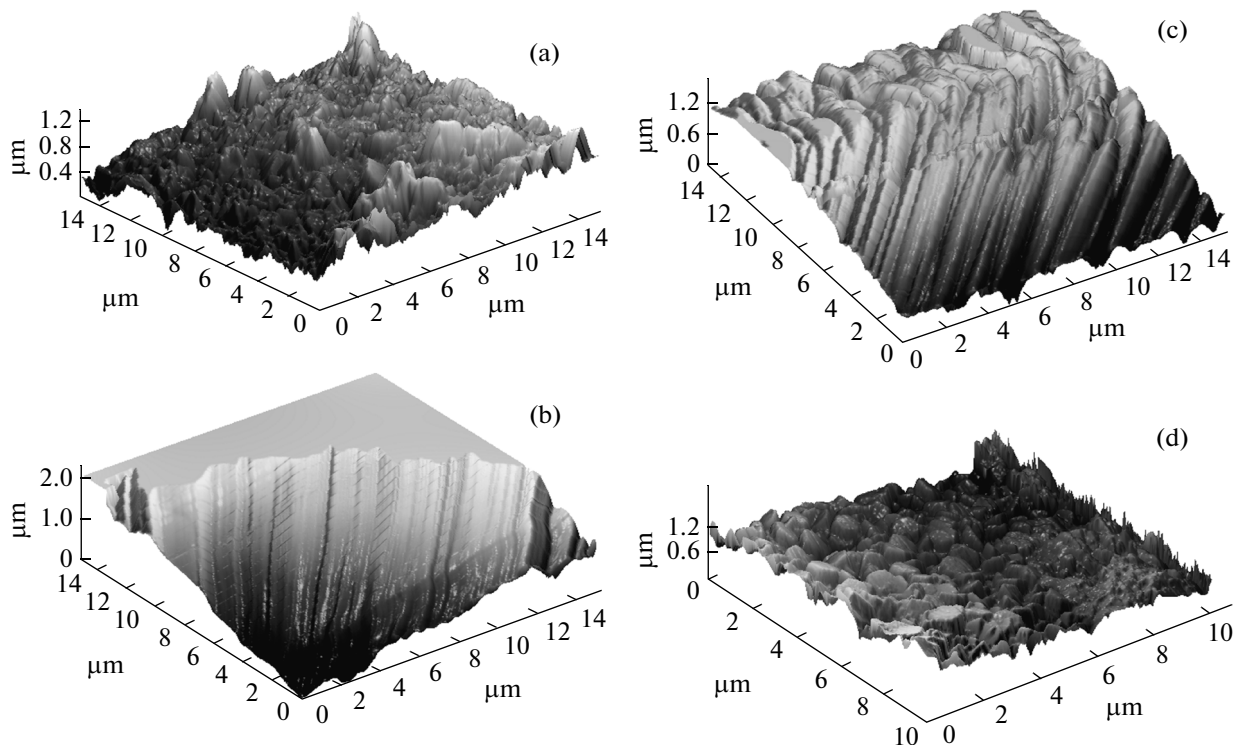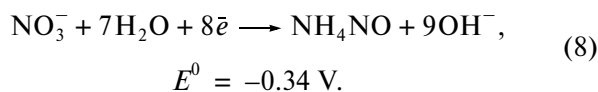
of reflections (002) is consistent with the formation of zinc oxide crystallites of the hexagonal modification, shaped as nanorods directed along the c axis. Furthermore, according to the published data [3, 4, 20], the formation of arrays of 1D ZnO nanostructures growing in the direction perpendicular to the substrate results from the preferred orientation of these crystallites in the (001) direction. The study of the texture of electrodeposited zinc oxide layers showed that ZnO layers grown at a constant substrate potential are almost untextured; there is insignificant preferred ori-
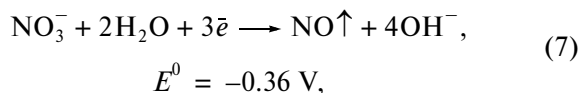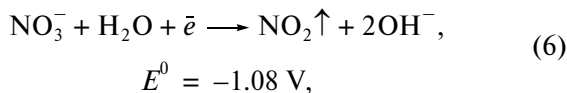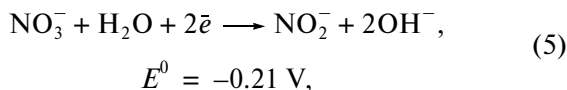
Fig. 7. AFM images of the surface of ZnO layers deposited in the (a) potentiostatic and (b) pulse modes at pulse frequencies $f =$ (b) 2, (c) 20, and (d) 200 Hz.

layer shown in Fig. 7b is formed by the longest and thinnest nanocrystallites. It is assumed that, in particular, the large length of ZnO nanocrystallites did not permit the use of the Williamson−Hall approximation method to analyze their substructure. At the same time, the small diameter of the nanowires fabricated at the cathode pulse frequency $f = 2$ Hz is the cause of the anomalously high optical transmittance in the visible region. We can see in Fig. 7d that zinc oxide crystallites of the hexagonal modification, shaped as stocky prisms up to 700 nm wide with hexagonal faces, are deposited at a potential pulse frequency of 200 Hz. In this case, some faces are parallel to the substrate plane ((002) texture); others are arranged to it at an angle corresponding to the (103) texture. We note that the most pronounced light scattering in the visible region is observed for the array of zinc oxide crystallites, fabricated at $f = 200$ Hz, which corresponds to the smallest values of T in Fig. 1. This is readily explained by the commensurability of the diameters of the crystallite end faces with the light wavelength.

4. DISCUSSION

Previously, based on the study of zinc oxide electrodeposition from an aqueous nitrate electrolyte [13], we detected that, if the cathode substrate potential is constant and equal to $U = -1.1$ V, electrochemical reactions can occur on the surface, whose standard potential E_0 is more positive than U, i.e.,

$$2H_2O + 2\bar{e} \longrightarrow H_2\uparrow + 2OH^-, \quad E^0 = -1.05 \text{ V}, \quad (4)$$

$$NO_3^- + H_2O + 2\bar{e} \longrightarrow NO_2^- + 2OH^-,$$
$$E^0 = -0.21 \text{ V}, \quad (5)$$

$$NO_3^- + H_2O + \bar{e} \longrightarrow NO_2\uparrow + 2OH^-,$$
$$E^0 = -1.08 \text{ V}, \quad (6)$$

$$NO_3^- + 2H_2O + 3\bar{e} \longrightarrow NO\uparrow + 4OH^-,$$
$$E^0 = -0.36 \text{ V}, \quad (7)$$

$$NO_3^- + 7H_2O + 8\bar{e} \longrightarrow NH_4NO + 9OH^-,$$
$$E^0 = -0.34 \text{ V}. \quad (8)$$

According to [13, 21], the interaction of zinc ions with hydroxyl groups results in the growth of zinc oxide layers on the cathode substrate surface,

$$Zn^{2+} + 2OH^- \longrightarrow Zn(OH)_2 \longrightarrow ZnO + H_2O. \quad (9)$$

The preferential growth of the (002) plane in the potentiostatic mode is prevented by gaseous hydrogen adsorption onto it. Therefore, the formed arrays of ZnO fragments are disordered and untextured (Fig. 7a).

Favorable conditions for the formation of arrays of filamentary crystals textured in the $\langle 001 \rangle$ direction are

created in the pulse electrolysis mode for the following reasons. At $U_{off} = -0.8$ V, hydrogen is not released at the cathode; therefore, growth of the zinc oxide (002) plane is not inhibited, and NO_3^- and Zn^{2+} ions diffuse to the cathode, which results in ZnO formation by reactions (5), (7), (8), and (9). In contrast, at $U_{on} = -1.4$ V, in addition to reactions (4)−(9), the cathodic reduction of zinc occurs by the reaction

$$Zn^{2+} + 2\bar{e} \longrightarrow Zn, \quad E^0 = -0.98 \text{ V}, \quad (10)$$
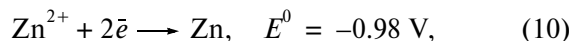
followed by the heterogeneous chemical reaction at U_{off},

$$Zn + NO_3^- + H_2O \longrightarrow NO_2^- + Zn(OH)_2$$
$$\longrightarrow NO_2^- + ZnO + H_2O. \quad (11)$$
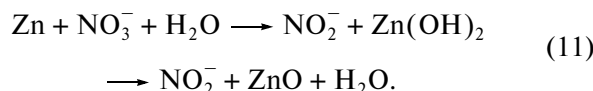
As a result, the growth rate of zinc oxide arrays increases during pulse electrolysis; therewith, preferential growth in the (002) plane is observed, i.e., zinc oxide filamentary crystals are formed.

We note that, according to [13] and the above results of the optical and structural studies, no metal zinc was detected in the zinc oxide layers grown in the potentiostatic mode at $U = -1.1$ V and in the pulse modes under consideration. From this, we can conclude that reaction (10) in the used zinc-ion diluted nitrate electrolyte occurs with significant overvoltage; therefore, the cathode potential at which this reaction can take place should be more negative than $U = -1.1$ V.

At the same time, when considering the effect of the cathode potential pulse frequency f on the structure, optical properties, and surface morphology of the ZnO layers, it should be taken into account that charge−discharge of the double electric layer (capacitive process) takes place along with electrochemical reduction (Faraday process) on the cathode in the case of pulse electrolysis [22]. According to [22], the effect of the capacitive process manifests itself as pulse shape distortion and amplitude decrease with increasing frequency. Thus, the higher f is, the less negative the actual cathode potential is during the pulse. Hence, at low frequencies, $f = 1-2$ Hz, zinc deposition occurs at the lowest negative potential, close to $U_{on} = -1.4$ V, i.e., with the maximum cathode overvoltage, under conditions of the formation of a large number of crystallization centers [22, 23]; therefore, the ZnO nanowire thickness does not exceed hundreds of nanometers (Fig. 7b). As the pulse frequency increases to $f = 20$ Hz, the actual cathode potential at U_{on} becomes more positive (although significantly exceeds -1.1 V), due to which the number of crystallization centers decreases, and zinc oxide filamentary crystals oriented in the $\langle 001 \rangle$ direction thicken to a few hundred nanometers (Fig. 7c). As the pulse frequency of the cathode potential increases to $f = 200$ Hz, the effect of the capacitive process on the cathode potential strengthens, and the actual cathode potential slightly exceeds -1.1 V at U_{on}. As a result, a small

number of zinc crystallization centers are formed, and the ZnO growth rate by reactions (10) and (11) decreases, which appears in the structure and properties of zinc oxide nanocrystal arrays as (002) plane growth inhibition, hence, a decrease in the texture perfection in the $\langle 001 \rangle$ direction and ZnO crystal thickening to 700 nm (Fig. 7d).

5. CONCLUSIONS

The systematic features of the growth of one-dimensional submicroscopic zinc oxide structures during pulse electrochemical deposition on a cathode substrate were determined by analyzing the electrochemical processes in an aqueous nitrate electrolyte and by the results of a study using X-ray diffraction, optical spectrophotometry, and atomic-force microscopy. Controlled growth of one-dimensional zinc oxide nanostructures was implemented using pulse electrolysis without organic or other surface-active additives in an electrolyte, i.e., without material contamination by impurities which can eventually (see [24]) cause the degradation of ZnO properties and even the destruction of zinc oxide nanocrystallite arrays. The possibility of fabricating arrays of ZnO nanowires of different geometrical shapes, perpendicular to the substrate surface, by varying the pulse frequency of the cathode substrate potential was shown.

REFERENCES

1. A. M. Bagamadova, B. M. Ataev, V. V. Mamedov, A. K. Omaev, and S. Sh. Makhmudov, Tech. Phys. Lett. **36**, 34 (2010).
2. C.-Y. Lu, S.-P. Chang, S.-J. Chang, T.-J. Hsuch, C.-L. Hsu, Y.-Z. Chiou, and I.-C. Chen, IEEE Sens. J. **9**, 485 (2009).
3. X. Hu, Y. Masuda, T. Ohji, and R. Kato, J. Chem. Soc. Jpn. **116**, 384 (2008).
4. X. Ju, W. Feng, X. Zhang, V. Kittichungchit, T. Hori, H. Moritou, A. Fujii, and M. Ozaki, Solar Energy Mater. Solar Cells **93**, 1562 (2009).
5. D. Pradhan and K. T. Leung, J. Phys. Chem. C **112**, 1357 (2008).
6. E. Michaelis, D. Wöhrle, J. Rathouysky, and M. Wark, Thin Solid Films **497**, 163 (2006).
7. O. Lupan, V. M. Guérin, I. M. Tiginyanu, V. V. Ursaki, L. Chow, H. Heinrich, and T. Pauporté, J. Photochem. Photobiol. A: Chem. **211**, 65 (2010).
8. M. Gupta, D. Pinisetty, J. C. Flake, and J. J. Spivey, J. Electrochem. Soc. **157**, D473 (2010).
9. H. Osaki, H. Yasuda, T. Watatsuli, Y. Kanemitsu, Y. Fukunaka, and K. Kuribayashi, Space Utiliz. Res. **24**, 27 (2008).
10. A. Kathalingam, M. R. Kim, Y. S. Chae, and J. K. Rhee, J. Korean Phys. Soc. **55**, 2476 (2009).
11. C. Coşkun, H. Güney, E. Gür, and S. Tüzemen, Turk. J. Phys. **33**, 49 (2009).
12. N. P. Klochko, Func. Mater. **14**, 343 (2007).
13. G. Khrypurov, N. Klochko, N. Volkova, V. Kopach, V. Lyubov, and K. Klepikova, in *Proceedings of the World Renewable Energy Congress* (Linköping, Sweden, 2011), 1002. PV.
14. A. Janotti and C. G. Walle, Rep. Progr. Phys. **72** (12), 1 (2009).
15. N. Stakti and P. S. Gupta, Appl. Phys. Res. **2** (1), 19 (2010).
16. S. S. Gorelik, L. N. Rasturguev, and Yu. A. Skakov, *X-Ray and Electron-Optical Analysis* (Metallurgiya, Moscow, 1970) [in Russian].
17. S. V. Tsybulya and S. V. Cherepanova, *Introduction into Structural Analysis of Nanocrystals* (Novosib. Gos. Univ., Novosibirsk, 2008) [in Russian].
18. *The Structure and Physical Properties of Solids. Laboratory Manual, The School-Book*, Ed. by L. S. Palatnik (Vishcha shkola, Kiev, 1983) [in Russian].
19. K. Govender, D. S. Boyle, P. B. Kenway, and P. O'Brein, J. Mater. Chem. **14**, 2575 (2004).
20. C. X. Xu, X. W. Sun, Z. L. Dong, G. P. Zhu, and Y. P. Cui, Appl. Phys. Lett. **88**, 093101 (2006).
21. Z. Shen, Y. Tang, L. Zhang, and L. Luo, Electrochim. Acta **51**, 5870 (2006).
22. M. S. Chandrasekar and M. Pushpavanum, Electrochim. Acta **53**, 3313 (2008).
23. B. B. Damaskin, O. A. Petrii, *Electrochemistry* (Vyssh. Shkola, Moscow, 1987) [in Russian].
24. Y. Masuda, N. Kinoshita, and K. Koumoto, J. Nanosci. Nanotechnol. **9**, 522 (2009).

Translated by A. Kazantsev